Glass transition in confined geometry

T. Fehr and H. Löwen
Sektion Physik der Universität München, Theresienstrasse 37, D-80333 München, Germany
(Received 2 May 1995)

Structural relaxation in an undercooled liquid confined between two parallel structureless plates is investigated by molecular dynamics simulations. It is found that the system exhibits a kinetic glass transition, detected as a crossover from hydrodynamic relaxation to a relaxation dominated by hopping processes. The kinetic transition occurs at significantly smaller densities than that of the bulk glass transition. In particular, the dependence of this density shift on the plate distance L is studied for systems involving 3 to 16 microscopic layers in between the plates. As a result, the density shift scales approximately proportionally to $\exp(-L/l_0)$ where l_0 is a microscopic length scale. Furthermore, the kinetic glass transition is a collective effect that occurs simultaneously in each layer.

PACS number(s): 64.70.Pf, 61.20.Ja

I. INTRODUCTION

A liquid confined between two parallel plates exhibits a marked layering on a molecular length scale. In such a confining geometry, the freezing transition is shifted to significantly higher temperature or lower pressure with respect to the bulk freezing point. In a thin confined liquid film dynamical and transport quantities also differ strikingly from their bulk values. This gives a first hint that also the kinetic glass transition [1], which is intimately connected with the temporal decay of dynamical correlations, may be drastically affected by a confining geometry. One may expect that the glass transition temperature T_g shifts to higher (and the density to smaller) values with respect to the bulk glass transition since the effective free volume per particle is reduced.

Although structural and dynamical properties of sheared confined liquid films have been extensively investigated during the past years using both experiments [2,3] and computer simulations [4–7], it is only recently that the nature of the liquid-to-glass transition in a finite geometry has been studied. The only substantial information stems from experiments on organic liquids confined in pores of a glassy material. These measurements offer, however, a rather puzzling picture: A finite-size-induced *decrease* of T_g was reported for *o*-terphenyl, benzyl [8], propylene [9], and for other organic liquids [10]. On the other hand, in accordance with intuition, quite a number of experiments report an increase of T_g [11–13]. Recently, the glass transition was also investigated for a liquid film [14] where again a depression of T_g was found.

Although there is an increasing theoretical understanding of the bulk glass transition using computer simulations [15,16] and mode coupling theory [17], no theoretical attempt was made to study a confined liquid near the glass transition until now. The only exception is the computer simulation of Ref. [18], where the influence of the finite box size with periodic boundary conditions on the glass transition was studied. However, this is of course not a suitable model for a situation where the liquid is confined by pores and between plates. The aim of the present paper is to introduce and to discuss a simple model of a binary liquid mixture confined between two parallel plates. Using extensive molecular dynamics simulations, we study how the bulk glass transition is influenced and altered by the presence of the walls. The motivation in doing so is twofold. First, since the model is relatively simple, one may expect to see the physically relevant principles of the shift in the glass transition temperature directly. Second, the bulk glass transition of the model is already known with high precision from extensive computer simulation studies by Hansen and coworkers [19–21]; see also [22]. Consequently, deviations from their results have to be attributed solely to confinement effects.

One of the main results of our computer simulation studies is that the kinetic glass transition in a highly layered liquid between parallel plates is a collective effect, i.e., each layer exhibits a dynamical anomaly at the same temperature and the glass transition does not occur layer by layer for a series of different temperatures. The dynamical anomaly consists in a sharp crossover from hydrodynamic relaxation to a relaxation dominated by thermal activated jump processes in each layer. This crossover is not connected to any discontinuity in the static structure; hence the glass transition is a pure dynamical effect. Another main result is that the glass transition temperature T_g shifts to significantly *higher* values compared to the bulk glass transition temperature. The results can also be translated into a reduction of the average density along an isotherm with respect to the bulk glass transition density. The density shift scales approximately proportionally to $\exp(-L/l_0)$, where L is the plate distance and l_0 is a constant.

The paper is organized as follows. In Sec. II the model is introduced. Then we describe briefly the simulation technique in Sec. III. Results for the density profiles and

the key dynamical correlation functions characterizing the glass transition are given in Secs. IV and V. We finish with a discussion and conclusion in Sec. VI.

II. MODEL

We consider a binary mixture of classical soft spheres at a given temperature T. Each species is characterized by a mass m_α, a soft sphere diameter σ_α, and a relative concentration $x_\alpha = N_\alpha/(N_1+N_2)$, N_α denoting the total number of particles ($\alpha=1,2$). The mutual interaction between the spheres is explicitly given by

$$V_{\alpha\beta}(r)=\epsilon\left[\frac{\sigma_{\alpha\beta}}{r}\right]^{12}, \quad \alpha,\beta\in\{1,2\} , \tag{1}$$

where r is the interparticle distance, ϵ sets the energy scale, and the additive diameter $\sigma_{\alpha\beta}$ is defined via

$$\sigma_{\alpha\beta}=(\sigma_\alpha+\sigma_\beta)/2, \quad \alpha,\beta\in\{1,2\} . \tag{2}$$

In order to facilitate a direct comparison with earlier bulk simulations, we chose the same parameters as in Refs. [20,21] throughout the paper: $m_2/m_1=2$, $\sigma_2/\sigma_1=1.20$, and $x_1=x_2=0.5$. With these parameters crystallization is practically inhibited completely on the time scale typically explored by a simulation. Furthermore, the length scale used in the paper is σ_1 and the time scale is

$$\tau=\left[\frac{m_1\sigma_1^2}{\epsilon}\right]^{1/2} . \tag{3}$$

Let us first briefly recapitulate the facts that are known in the bulk soft sphere mixture. First, all structural properties depend only on the dimensionless coupling constant Γ, which is defined as

$$\Gamma=\rho_x^*(T^*)^{-1/4} . \tag{4}$$

Here the scaled particle density ρ_x^* is

$$\rho_x^*=(N_1+N_2)\sigma_x^3/V , \tag{5}$$

where V denotes the total volume of the system, σ_x is given via the relation

$$\sigma_x^2=x_1^2\sigma_1^3+2x_1x_2\sigma_{12}^3+x_2^2\sigma_2^3 , \tag{6}$$

and the scaled temperature T^* is

$$T^*=k_BT/\epsilon , \tag{7}$$

where k_B is Boltzmann's constant.

Second, in a pioneering computer simulation study of the bulk glass transition, Roux, Barrat, and Hansen [20,21] found that the binary soft sphere mixture exhibits a kinetic glass transition in the supercooled liquid phase at a coupling constant

$$\Gamma=\Gamma_g^{(0)}=1.45\pm0.01 , \tag{8}$$

which readily fixes the bulk glass transition temperature $T_g^{(0)}$ via (4) and (7). The glass transition was detected by observing a change in the relaxation mechanism as visualized in the Van Hove correlation functions

$$G_s^{(\alpha)}(r,t)=\frac{1}{N_\alpha}\left\langle\sum_{j=1}^{N_\alpha}\delta(\vec{r}-\vec{r}_j^{\,\alpha}(0)+\vec{r}_j^{\,\alpha}(t))\right\rangle , \quad \alpha,\beta\in\{1,2\} , \tag{9}$$

where $\vec{r}_j^{\,\alpha}(t)$ denotes the position of particle j of species α at time t and $\langle\ \rangle$ is a canonical average. For temperatures higher than $T_g^{(0)}$, the relaxation of $G_s^{(\alpha)}(r,t)$ has a strong hydrodynamic character; this means that the Van Hove functions reach their hydrodynamic long-time limit

$$G_s^{(\alpha)}(r,t)\simeq\frac{1}{(4\pi D_\alpha t)^{3/2}}\exp\left[-\frac{r^2}{4D_\alpha t}\right] \tag{10}$$

quite rapidly. In (10), D_α denotes the long-time self-diffusion coefficient of particle species α. On the other hand, for $T<T_g^{(0)}$ the relaxation in $G_s^{(\alpha)}(r,t)$ occurs mainly by thermal activated jumps along a nearest-neighbor distance $a=\rho^{-1/3}$, where $\rho=(N_1+N_2)/V$ is the total number density, V denoting the total volume of the system. The jump processes cause a shoulder in $G_s^{(\alpha)}(r,t)$ at $r\simeq a$ for fixed large times t. This change in relaxation occurs in a very narrow temperature interval and is interpreted as a kinetic glass transition. Furthermore, the following points were carefully checked in Refs. [20,21], revealing that the glass transition is an *intrinsic* property of the supercooled fluid.

(i) As any static correlations, the kinetic glass transition depends only on Γ.

(ii) The kinetic glass transition is independent of the cooling rate provided this rate is gentle enough.

(iii) Freezing in of dynamical correlations occurs for both types of spheres at the same coupling Γ.

(iv) The location of the kinetic glass transition does not depend on the mass ratio m_2/m_1.

Let us now discuss how to introduce a confining wall in the model. Effects of confinement are most conveniently described by taking the walls as fixed and inert, acting on the particles of species α as an external potential $V_\alpha^{(\text{ext})}(\vec{r})$. Of course, in the bulk, $V_\alpha^{(\text{ext})}(\vec{r})=0$. Two parallel walls are modeled by choosing

$$V_\alpha^{(\text{ext})}(\vec{r})=\frac{\pi\rho\epsilon[(\sigma_{12}+\sigma_\alpha)/2]^{12}}{45}\times\left[\frac{1}{(z+L/2)^9}-\frac{1}{(z-L/2)^9}\right] , \tag{11}$$

where z is the coordinate perpendicular to the plates and σ_{12} is defined via (2). By introducing the external potential (11), the system is confined to the finite interval $-L/2<z<L/2$, where L is the plate distance. This then causes a strong layering in the liquid between the plates.

The motivation to take the expression (11) stems from the fact that $V_\alpha^{(\text{ext})}(\vec{r})$ is exactly the potential of a semi-

infinite homogeneous bulk of fixed spheres with the same relative concentration and total density ρ as in the confined system. This total density ρ is defined in the confined system via

$$\rho=(N_1+N_2)/(LL_{\parallel}^2) , \tag{12}$$

where $LL_{\parallel}^2$ is the total volume accessible by the particles and $L_{\parallel}$ denotes the system size in lateral direction. In fact, $L_{\parallel}$ may be thought of as a macroscopic length or the microscopic size of a finite simulation box with periodic boundary conditions in lateral directions. In analogy to the bulk expression (4), we define the coupling parameter Γ in the confined system by

$$\Gamma=\rho\sigma_x^3(T^*)^{-1/4} . \tag{13}$$

Since the external potential (11) depends only on z, the walls do not carry any lateral structure.

III. COMPUTER SIMULATION OF THE GLASS TRANSITION

The finite-difference version of the Newtonian equations of motion are integrated using a Verlet scheme of standard constant-temperature molecular dynamics [23]. The simulation box was rectangular, consisting of a square with periodic boundary conditions in lateral directions. The total number of particles used in the simulation was $N_1+N_2=500$, i.e., $N_1=250$ and $N_2=250$. It was carefully checked that the time step Δt was small enough; for the parameters used in the simulations $0.005\tau\leq\Delta t\leq 0.015\tau$ was chosen to be slightly depending on temperature.

For a given wall separation L the system was gently cooled down from high temperatures to temperatures in the neighborhood of the kinetic glass transition while keeping the total density fixed to $\rho\sigma_1^3=1$. Near the glass transition one run typically involved 10^5 equilibration time steps and 10^5 steps to collect statistics for static and dynamic correlations. One typical cooling rate is shown in Fig. 1, where the coupling parameter Γ is plotted versus total time t. In fact, in Fig. 1, one sees a whole series of runs defining one cooling history. The end configuration of a run was successively used as a starting configuration of a slightly cooled run. Three different cooling curves are shown: The dashed line corresponds to the temperature prescribed in the framework of constant-T molecular dynamics. As it should be, the temperature that is actually realized by the system (solid line) is then very close to the prescribed temperature. Finally, the dash-dotted line is the corresponding coupling Γ in one layer lying near $z=0$ in between the walls. Since there are large fluctuations in the particle number within one single layer (the precise definition of this quantity will be given later in Sec. IV), the effective averaged coupling in this layer can significantly deviate from the global system-averaged value prescribed within the simulations.

Generally, it was found that a larger equilibration time is needed for a confined system than that needed for bulk equilibration. Consequently, the cooling rate had to be significantly smaller than that in Refs. [20,21]. Also the sensitivity of the results to a different cooling rate was checked by enhancing and lowering it by a factor 2. No changes were observed for the location of the glass transition and the static correlations while the long-time dynamical correlations were qualitatively similar but differ quantitatively due to lack of statistics. This fact, however, will not affect any conclusion in the paper.

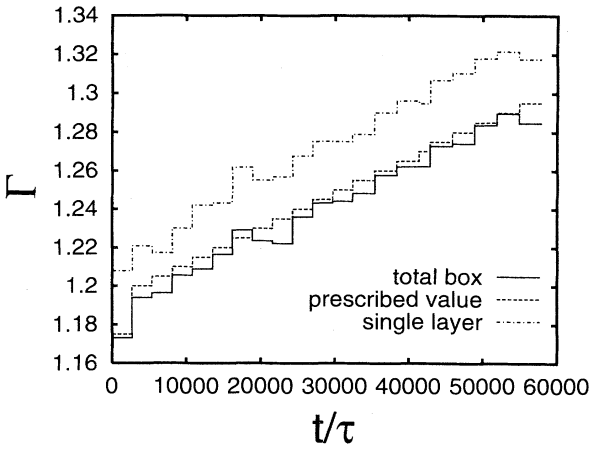

FIG. 1. Cooling history for series C of the simulation. The coupling parameter Γ is shown versus reduced time t/τ: prescribed value, dashed line; actual average value of the coupling in the total simulational box, solid line; coupling in one layer in between the walls, dash-dotted line.

Altogether five different sets $A-E$ of runs were done for different plate separations L; their parameters are summarized in Table I. These series involve wall separations ranging from $L=5\sigma_1$ to $14.6\sigma_1$. Each series corresponds to one cooling history comprising 15–30 single runs of different temperature [24].

IV. DENSITY PROFILES BETWEEN THE WALLS

Before discussing dynamical relaxation, let us first focus on results for static quantities. The microscopic layering in a liquid confined between two parallel plates manifests itself directly as oscillations in the one-particle density profiles of both particles species, which are defined via

TABLE I. Lateral box length $L_{\parallel}/\sigma_1$, plate distance L/σ_1, number of microscopic layers n_l, and coupling parameter of the glass transition Γ_g for the different series of runs $A-E$.

Run	$L_{\parallel}/\sigma_1$	L/σ_1	n_l	Γ_g
A	10.00	5.00	5	1.07±0.01
B	7.94	7.94	8	1.21±0.02
C	6.93	10.40	11	1.25±0.02
D	6.30	12.60	14	1.31±0.02
E	5.85	14.62	16	1.37±0.01

$$\rho^{(\alpha)}(z)=\left\langle \sum_{i=1}^{N_\alpha} \delta(\vec{r}-\vec{r}_i^{(\alpha)}) \right\rangle, \quad \alpha=1,2 \ . \tag{14}$$

In the (inhomogeneous) fluid phase, this quantity depends only on the coordinate z perpendicular to the plates. An example is shown in Fig. 2, where the series A and $\Gamma=1.070$ is taken. One sees that five layers are built up between the walls while the density distribution of the large spheres follows closely that of the small spheres, except in the outermost layers, which prefer the large spheres. Strictly speaking the density profile should be inflection symmetric around $z=0$; the small asymmetry stems from the effect that the system has not been completely equilibrated near the wall contact.

The number of layers is entirely fixed by the wall separation and independent of temperature. This is demonstrated in Fig. 3, where the profile of the total density

$$\rho(z)=\rho^{(1)}(z)+\rho^{(2)}(z) \tag{15}$$

is plotted for different runs from series A as a function of Γ. For high temperature ($\Gamma=0.499$) the third layer in between the walls is hardly visible, i.e., the system practically exhibits structural bulk properties around $z=0$. For low temperatures close to the kinetic glass transition ($\Gamma=1.070$), the layering is very sharp. This holds true even for such large wall separations with 15 layers (series E), the largest value explored in this paper. Consequently, for the values of L examined in our study, there are still strong anisotropic correlations near $z=0$. Of course, in the extreme limit of large L, these structural anisotropies vanish since the amplitudes of the density profiles decay exponentially as a function of wall distance. The number of layers n_l corresponding to each set of simulations is given in Table I.

It was always observed during the gentle cooling series of the simulations that the density profiles depend smoothly on temperature variation. For instance, in Fig. 3, a slight change in Γ from $\Gamma=1.062$ to 1.070 (which turns out to be very close to the kinetic glass transition in fact) induces only a small change in $\rho(z)$. This observation has two implications. First, it strongly indicates that there is no sudden in-plane freezing that would manifest itself as a discontinuity in the density profile as a function of temperature (see Ref. [25] for a discussion of such a first-order in-plane freezing in sedimentation density profiles). Second, we shall see in Sec. V that the *dynamical* relaxation will drastically slow down for a very small temperature reduction, which will be interpreted as a kinetic glass transition. The continuity of $\rho(z)$ at the glass transition implies that the transition is of a purely dynamical nature. This is in agreement with the common view on the bulk glass transition within mode coupling theory [17], where continuous liquid structural correlations yield a discontinuous dynamical behavior.

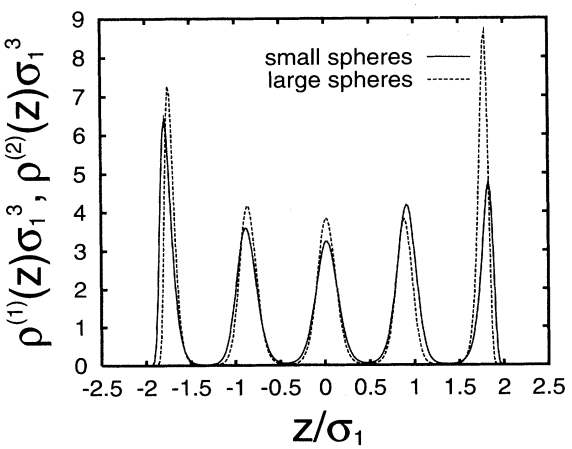

FIG. 2. Partial density profiles of the small spheres $\rho^{(1)}(z)\sigma_1^3$ (dashed line) and for the large spheres $\rho^{(2)}(z)\sigma_1^3$ (solid line) versus z/σ_1 for series A ($\Gamma=1.070$).

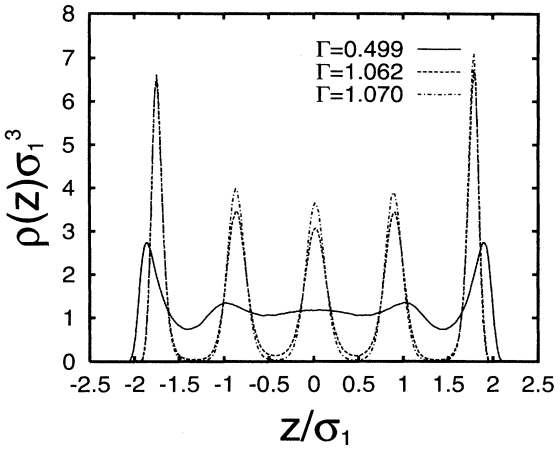

FIG. 3. Total density profile $\rho(z)\sigma_1^3$ belonging to run series A for three different couplings: $\Gamma=0.499$ (solid line), $\Gamma=1.062$ (dashed line), and $\Gamma=1.070$ (dash-dotted line).

The total density profile $\rho(z)$ can serve in a natural way for a definition of the total layer thickness. For a number of n_l layers, let $z_1^m<z_2^m<\cdots<z_{n_l-1}^m$ denote the positions of the *minima* of the density profile $\rho(z)$. Then the thickness of the layer i ($1\le i\le n_l$) is $z_i^m-z_{i-1}^m$ with $z_0^m\equiv -L/2$ and $z_{n_l}^m\equiv L/2$. On the z axis the ith layer falls in the interval $z_{i-1}^m\le z<z_i^m$. Consequently, the average number of particles $\mathcal{N}_i$ per area in the ith layer is given by

$$\mathcal{N}_i/L_\parallel^2=\int_{z_{i-1}^m}^{z_i^m} dz\,\rho(z) \ . \tag{16}$$

During the simulation we did not observe a full segregation or phase separation of the large and small spheres even for temperatures near the glass transition. This is based on an analysis of particle configurations during the simulation. In a typical configuration of the outermost layers, the particles are distributed on a matrix that locally exhibits the structure of a triangular lattice. Near the kinetic glass transition such a configuration is depicted in Fig. 4. Although the snapshot looks like a triangular

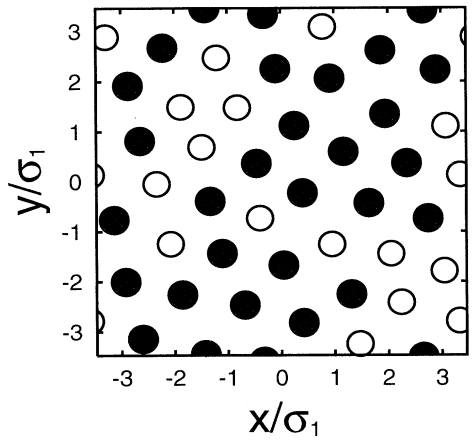

FIG. 4. Snapshot of the particle positions in an outermost layer (xy plane) near the wall for series C ($\Gamma=1.274$). The in-plane coordinates of small spheres are depicted by open circles, those of the large spheres by full dark circles. The size of the square is the lateral box length $L_{\parallel}$ of the simulation.

crystal, there is no full translational long-range order within the finite lateral box cell of the simulation, i.e., the system does not freeze into a laterally structured phase. Still, Fig. 4 shows that there are considerable static in-plane correlations within one layer. One also sees a significant clustering within the plane, but no complete phase separation.

V. SLOWING DOWN OF DYNAMICAL CORRELATIONS

A. Van Hove correlation functions

As discussed earlier, a sensitive dynamical diagnostics for the kinetic bulk glass transition is provided by the relaxation mechanism as visualized in the Van Hove functions $G_s^{(\alpha)}(r,t)$, which are defined by Eq. (9) [20]. We have also investigated this key quantity for the confined liquid. In order to resolve the dynamical behavior layer by layer, it is convenient to introduce the Van Hove functions $\overline{G}_s^{(\alpha)}(r,z_1,z_2,t)$ projected onto the planar coordinates x and y ($r=\sqrt{x^2+y^2}$) for particle trajectories whose z coordinates start and end in the interval $z_1 \le z < z_2$. These functions have also been analyzed in the context of the kinetic glass transition in strictly two-dimensional fluids [26,27]. Their explicit definition is given by

$$\overline{G}_s^{(\alpha)}(r,z_1,z_2,t) = \left\langle \frac{L_{\parallel}^2\sigma_1}{\overline{N}_\alpha} \sum_{j=1}^{N_\alpha} \delta(x-x_j^{(\alpha)}(0)+x_j^{(\alpha)}(t)) \times \delta(y-y_j^{(\alpha)}(0)+y_j^{(\alpha)}(t)) \right\rangle , \quad (17)$$

where the sum in (17) is restricted to

$$z_1 \le z_j^{(\alpha)}(0), \quad z_j^{(\alpha)}(t) < z_2, \quad \alpha=1,2 . \quad (18)$$

In (17), $\overline{N}_\alpha$ denotes the actual number of terms in the restricted sum. The projected Van Hove function of the ith layer is then obtained by setting $z_1=z_{i=1}^m$ and $z_2=z_i^m$.

For the run series C where the density profile consists of 11 layers, the projected Van Hove function for the small particles is shown in Figs. 5(a)–5(c) for different

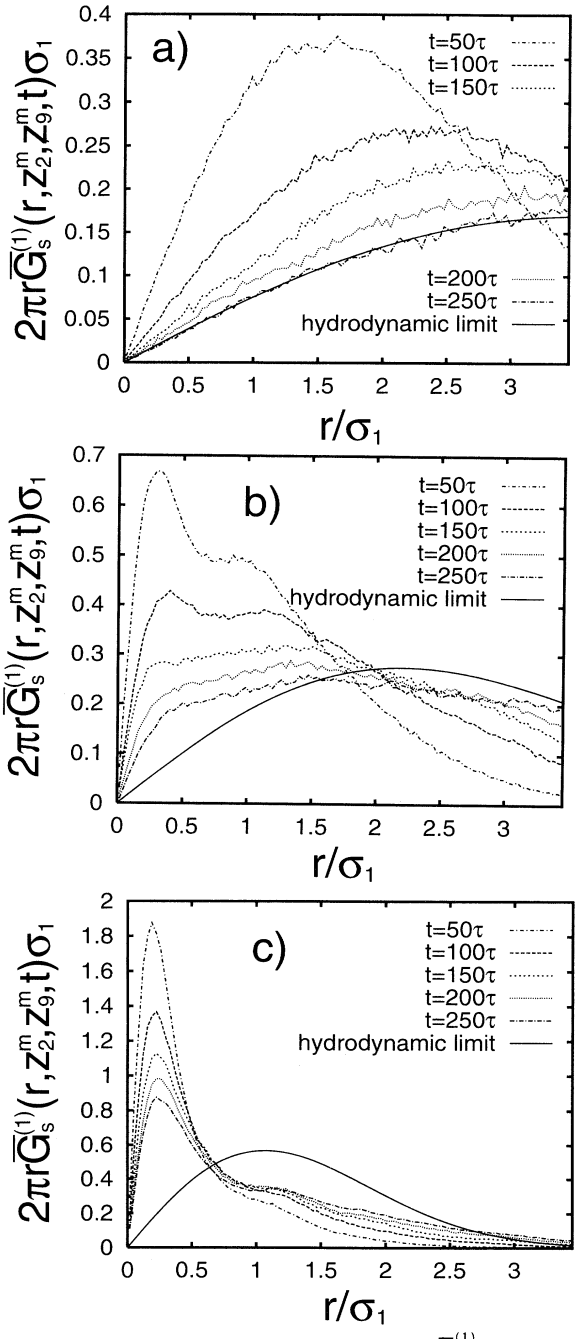

FIG. 5. Van Hove correlation functions $\overline{G}_s^{(1)}(r,z_2^m,z_9^m,t)$ for the third to ninth layer versus r/σ_1 for different times $t/\tau=50,100,150,200,250$ (run series C). The hydrodynamic limit for $t/\tau=250$ is also shown (solid line). (a) $\Gamma=1.173$, (b) $\Gamma=1.217$, and (c) $\Gamma=1.248$.

couplings Γ at various times t. The z coordinate is restricted between the third and the ninth layer. For a large time t, the hydrodynamic limit

$$\frac{1}{4\pi D_\alpha(t)t}\exp\left[-\frac{r^2}{4D_\alpha(t)t}\right] \tag{19}$$

is also shown with a self-diffusion coefficient $D_\alpha(t)$ obtained from the corresponding mean-square displacement by Einstein's formula in two dimensions

$$D_\alpha(t)=\frac{1}{4t}\left\langle\frac{1}{N_\alpha}\sum_{j=1}^{N_\alpha}\{[x_j^{(\alpha)}(t)-x_j^{(\alpha)}(0)]^2 +[y_j^{(\alpha)}(t)-y_j^{(\alpha)}(0)]^2\}\right\rangle . \tag{20}$$

For $\Gamma=1.173$ [Fig. 5(a)], the relaxation quickly reaches its hydrodynamic limit within the time explored by the simulation ($t=250\tau$). It is thus still a fluid. If Γ is enhanced to $\Gamma=1.217$ [Fig. 5(b)], there is a secondary peak visible for smaller time, indicating that jump processes do play already a role and that the system is close to the kinetic glass transition. Still the system reaches its hydrodynamic limit at $t\simeq 250\tau$, however, within a much larger relaxation time than that in Fig. 5(a). A clear-cut distinction between the two peaks is seen for $\Gamma=1.248$ in Fig. 5(c), where the system does not relax towards its hydrodynamic limit within a large time of several hundreds of τ. This implies that the relaxation time has dramatically increased upon a slight change in temperature and that the kinetic glass transition has occurred. If Γ is again slightly enhanced, the system is completely frozen on the time scale explored by the simulation. From the given data we can thus estimate the kinetic glass transition to occur in a relatively narrow temperature interval at $\Gamma=\Gamma_g=1.24\pm 0.02$. This value is significantly smaller than its bulk value $\Gamma_g^{(0)}=1.45\pm 0.01$, which means that the glass transition temperature is shifted to *higher* values with respect to the bulk.

By an extensive analysis of the Van Hove functions we find the following results.

(i) The kinetic glass transition occurs for the large spheres and for the small spheres at the same temperature and value, respectively, of the coupling constant Γ. This result was also obtained for the bulk simulation [20] and carries over simply to the confined-fluid case.

(ii) The kinetic glass transition as detected by a dynamic anomaly in the Van Hove correlation functions occurs at the same temperature for each layer. This important result implies that the transition is not a series of transitions starting from the outermost layers and then growing layer by layer into the bulk, but contrarily is a *collective* effect. Though the layers are well separated, they still interact with each other and freeze at the same temperature into a glass. This is demonstrated in Figs. 6(a)–6(c), where the Van Hove function for the outermost layer is shown for the same parameters as in Figs. 5(a)–5(c). Generally speaking, the relaxation in the outermost layer is considerably slower than that in the intermediate layer. However, the dramatic *change* in the relaxation time towards the hydrodynamic limit occurs at the same value of the coupling. In Fig. 6(a) the outermost layer is fluidlike, while for Fig. 6(c) it is nearly completely frozen in. This corresponds completely to the relaxation in the intermediate layers as visualized in Figs. 5(a)–5(c).

(iii) The glass transition temperature increases for de-

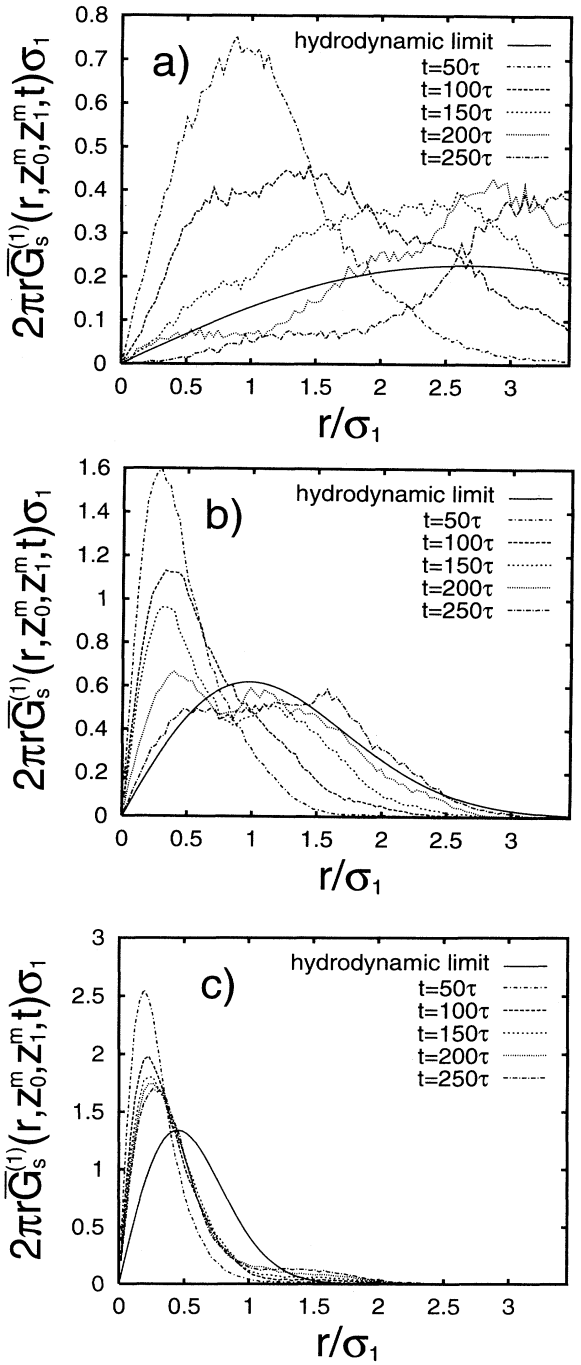

FIG. 6. Same as Fig. 5 but now for the outermost layer. The Van Hove correlation function $\bar{G}_s^{(1)}(r,z_0^m,z_1^m,t)$ is shown versus r/σ_1 for different times $t/\tau=50,100,150,200,250$ (run series *C*) including the hydrodynamic limit (solid line). (a) $\Gamma=1.173$, (b) $\Gamma=1.217$, and (c) $\Gamma=1.248$.

creasing wall separation L. The results are discussed in detail in Sec. V D.

(iv) The glass transition becomes sharper (i.e., it occurs in a smaller temperature interval) if the distance L between the plates decreases. In order to see this, we have plotted the Van Hove correlation function of the series A in Figs. 7(a) and 7(b), corresponding to the intermediate (third) layer. From $\Gamma=1.063$ [Fig. 7(a)] to $\Gamma=1.070$ [Fig. 7(b)] there is a sudden frozen-in process visible where the relaxation mechanism in the layer changes from hydrodynamic behavior to that mediated by thermal activated jump processes. The jumps manifest themselves as a strong secondary peak at $r/\sigma_1\simeq 1$. This implies that particle exchange processes between neighboring particles in the layer are the dominant contributions to the relaxation. For large times in Fig. 7(b), there is even a third peak at about $r/\sigma_1\simeq 2$, which is composed of two such nearest-neighbor jumps.

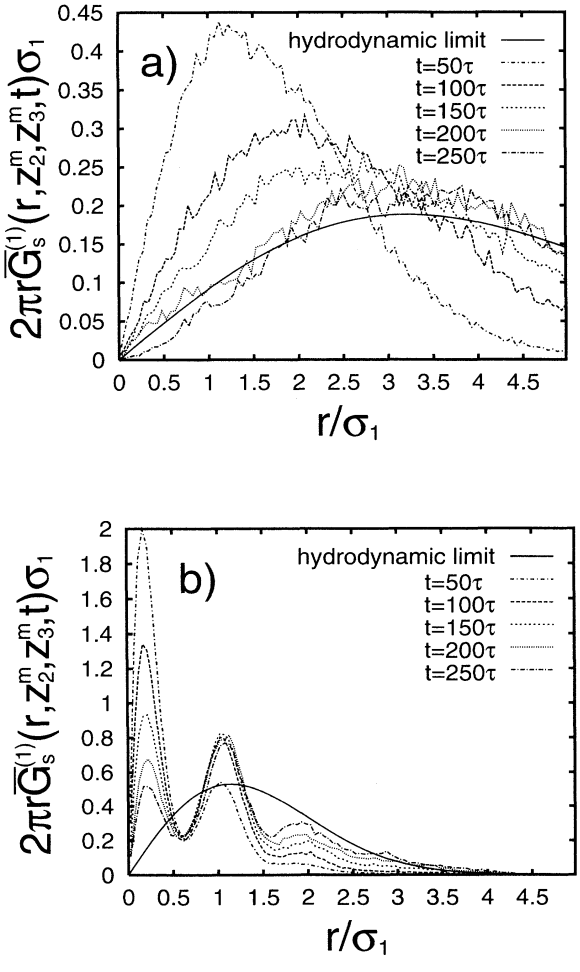

FIG. 7. Same as Fig. 5 but now for the run series A and the intermediate third layer. The Van Hove correlation function $\bar{G}_s^{(\alpha)}(r,z_2^m,z_3^m,t)$ is shown versus r/σ_1 for different times $t/\tau=50,100,150,200,250$ including the hydrodynamic limit (solid line). (a) $\Gamma=1.063$ and (b) $\Gamma+1.070$.

B. Particle trajectories

A further direct diagnostics for the dominant relaxation mechanism is a study of particle trajectories. Doing this near the kinetic glass transition, the following picture has emerged by our simulations. In the fluid case, the particles diffuse hydrodynamically within the layers and occasionally jump in z direction from one layer to another one. At the glass transition the jumps in z direction are highly suppressed and in the layer parallel to the walls activated jump processes are visible. In Fig. 8 one particle trajectory projected to the yz plane as well as to the xy plane is shown a bit below the glass transition temperature. While jump processes with a typical nearest-neighbor spacing are seen in the xy plane, the motion is practically frozen in the z direction, i.e., hopping in the z direction is a very rare event.

C. Self-diffusion

Using Einstein's formula (20) we can define a time-dependent diffusion coefficient $D_\alpha(t)$ $(\alpha,\beta=1,2)$. The corresponding generalization for diffusion in the ith layer is

$$D_\alpha^{(i)}(t)=\frac{1}{4t}\left\langle\frac{1}{\bar{N}_\alpha}\sum_{j=1}^{N_\alpha}\{[x_j^{(\alpha)}(t)-x_j^{(\alpha)}(0)]^2+[y_j^{(\alpha)}(t)-y_j^{(\alpha)}(0)]^2\}\right\rangle , \tag{21}$$

where the sum is again restricted by the condition (18). The quantity $D_\alpha^{(3)}(t)$ is plotted for a fixed large time t versus Γ in Fig. 9 for series A. As expected, near the kinetic glass transition, the diffusion drastically drops to very small values (note the logarithmic scale for $D_\alpha^{(3)}(t)$ in Fig. 9). The location of the glass transition may therefore also be determined by a drastical reduction of long-time diffusion. Figure 9 shows that this definition is

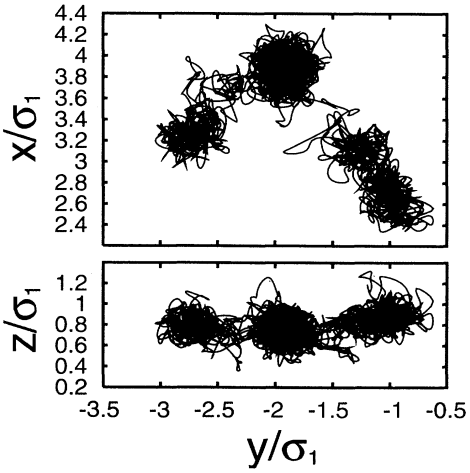

FIG. 8. Trajectory of a small sphere projected to the xy and the yz plane from series C with $\Gamma=1.274$. The total amount of time in generating this trajectory was 225τ.

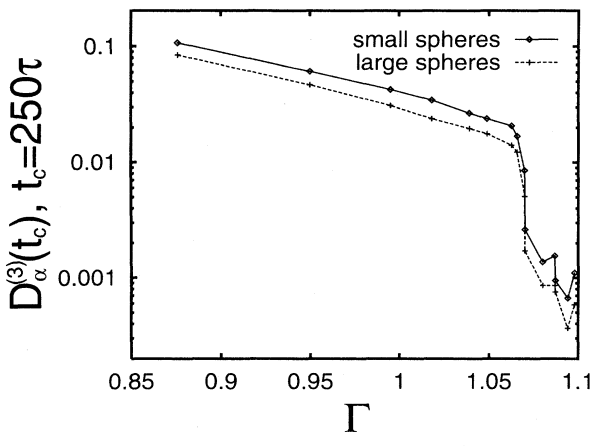

FIG. 9. Diffusion coefficient $D_\alpha^{(3)}(t_c)$ in the third layer of series A versus coupling constant Γ for a fixed time $t_c=250\tau$. Both cases $\alpha=1,2$ are shown. Note the logarithmic scale for $D_\alpha^{(3)}(t)$.

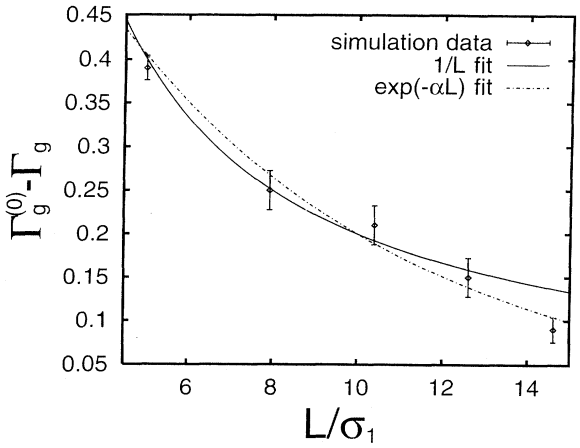

FIG. 10. Shift of the glass transition density $\Gamma_g^{(0)}-\Gamma_g$ versus plate distance L/σ_1. The data of the simulation including their error bars are shown together with the one-parameter fit proportional to $1/L$ and the two-parameter exponential fit proportional to $\exp(-\alpha L)$.

equivalent to that formerly discussed with the help of the Van Hove correlation functions. In both cases, $\Gamma_g=1.070\pm0.005$.

The layers near the wall exhibit a much slower diffusion [24]. However, the *change* in the diffusion coefficient happens at the same coupling as that belonging to an intermediate layer.

D. Shift of the glass transition

Using the same diagnostics as in Sec. V A and V C, the glass transition temperature was determined for five different wall separations L (series $A-E$). The results for the coupling Γ_g, where a slowing down of the dynamical correlations was observed, are summarized in Table I. In any case there was a shift towards higher temperatures (lower density) with respect to the bulk glass transition temperature (density). In order to evaluate these data quantitatively we have tried to fit them by relatively simple laws. A good one-parameter fit was obtained using an inverse power law

$$\Delta\Gamma_g\equiv\Gamma_g^{(0)}-\Gamma_g=l/L\ , \tag{22}$$

where $l=2.00\sigma_1$ is a microscopic length scale. Admitting two fit parameters A_0 and l_0, we found that an exponential law fits the data well

$$\Delta\Gamma g\equiv\Gamma_g^{(0)}-\Gamma_g=A_0\ \exp(-L/l_0)\ , \tag{23}$$

with $A_0=0.818$ and $l_0=7.09\sigma_1$.

In Fig. 10 we have plotted ΔT_g versus L together with the fits of (22) and (23). While the one-parameter fit fails to describe all data within the error bars, the exponential law (23) fits the data quite well. Since the glass transition only depends on Γ, (23) implies that the *density reduction scales with* $\exp(-L/l_0)$. Of course, as our data set is limited, this does not rule out other relations between $\Delta\Gamma_g$ and L.

It is instructive to compare our numerical data with recent theoretical predictions. Bocquet and Barrat have proposed a phenomenological hydrodynamic approach for correlation functions of confined fluids [28,29]. On the other hand, a relatively simple mode coupling theory for the bulk glass transition was proposed some years ago by Geszti [30], who viewed the glass transition as mediated by a viscosity-feedback mechanism. If Geszti's theory is combined with the hydrodynamic approach of Bocquet and Barrat, one gets a simple theory for the glass transition in a confined liquid [31]. Within this theory the shift in the glass transition temperature with respect to the bulk value scales with the plate distance L in the form

$$T_g-T_g^{(0)}=\frac{\overline{A}\ln(L/\sigma)+\overline{B}}{L}\ , \tag{24}$$

where $\overline{A}>0$ and $\overline{B}$ are constants that can be related to bulk correlations and σ is an arbitrary microscopic length scale. One should note that the expression (24) is only valid asymptotically for very large L. In particular, the oscillations in the density profiles between the plates should have been decayed to zero in between the plates near $z=0$, which implies that both plates are practically decoupled. Since in our simulations even for the largest plate distance there are still strong oscillations in the density profile, one cannot directly compare (24) with our results. However, it is tempting to check whether the expression (24) remains valid for smaller L. In order to perform this check, we have plotted $L(T_g-T_g^{(0)})$ versus $\ln(L/\sigma_1)$ in Fig. 11. If (24) would be true, all the data should fall on a straight line. The plot of Fig. 11, however, reveals that the expression (24) breaks down for lengths L of few microscopic spacings, but a linear relation seems to be valid for larger L. Hence Eq. (24) can be used only to describe the data for relatively large L comprising roughly at least ten microscopic layers.

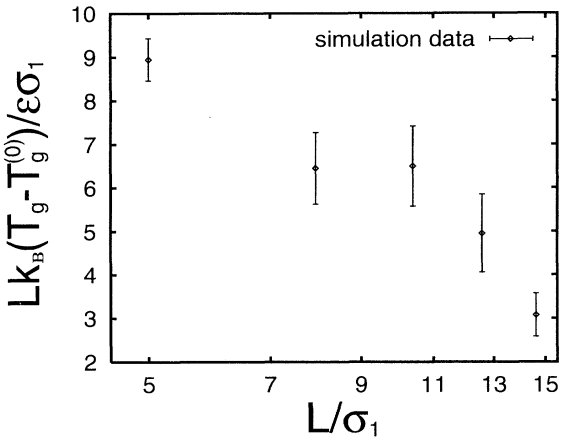

FIG. 11. Shift in the glass transition temperature times plate distance $Lk_B(T_g - T_g^{(0)})/\epsilon\sigma_1$ versus L/σ_1.

VI. CONCLUSIONS AND DISCUSSIONS

In conclusion, we have investigated the glass transition for a fluid confined between parallel plates. It occurs at significant higher temperatures (lower densities) than the bulk glass transition. For example, if the system consists of five layers, the shift $\Delta T_g/T_g^{(0)}$ is about 3.3, which corresponds to a density reduction of 26%. Furthermore, we presented evidence that the glass transition between plates is a collective effect of all layers between the plates.

We close with some remarks on the possibility of an experimental observation of the glass transition in a confined fluid. First of all, we remark that the present model is designed for fragile glass formers carrying only very weak chemical bonds in the fluid phase. An excellent experimental realization of such a fragile glass former on a mesoscopic length scale are colloidal suspensions of spherical macromolecules [16]. The effective interaction between sterically stabilized index-matched suspensions is governed by excluded-volume effects and a hard-sphere model is appropriate to describe the interaction. The bulk glass transition in sterically stabilized suspensions has been extensively studied by dynamical light scattering (see, e.g., [32]) and good overall agreement was obtained by comparing the results with that obtained from mode coupling theory for hard spheres. Colloidal suspensions can also be confined between parallel glass plates [33–36] and watched directly in real space by optical microscopy and digital image processing [37]. In particular, it should be possible to watch the glass transition by resolving the long-time dynamics. The distance between the plates can be varied easily and thus the structural and dynamical correlations can be studied as a function of L. Of course one should bear in mind that the interaction between colloids is not well described by the inverse power law (1), but is rather hard-sphere-like for sterically stabilized suspensions and Yukawa-like for charge-stabilized suspensions [38]. Also the dynamics are Brownian rather than Newtonian. Recent studies [39,40], however, indicate that the long-time dynamics relevant for the location of the kinetic glass transition is not affected by the short-time dynamics. Therefore all *qualitative* features of the glass transition in a confined fluid obtained by our simulation should persist for colloidal suspensions. In particular, the scaling of the density reduction with $\exp(-L/l_0)$ [i.e., Eq. (23)] can be tested using sterically stabilized suspensions between glass plates. Hence experiments on several layers of colloidal particles confined between parallel plates are highly desirable in order to check our theoretical predictions.

The experiments mentioned in the Introduction use organic complex liquids. It is obvious that these liquids are not well described by our soft-sphere model. The shift of the glass transition in the confined liquid towards lower temperature with respect to the bulk can be explained by the complex nature of the liquids and/or by details of the wall or the interface built up on the porous medium. A wall roughness may again influence the glass transition and it is conceivable that for a more complicated wall-particle interaction a depression of T_g is achieved. One simple example, again in the context of simple liquids, may help to understand this. Consider a wall-particle interaction that is strongly repulsive but also has an attractive part near the wall. In the attractive well, a dense layer of particles will accumulate (and even freeze into a triangular crystal) in equilibrium. Hence the rest of the system becomes less dense. It is now strongly expected that in this remaining layers the glass transition is shifted to lower temperature since the density is smaller. Hence, at least in principle, a depression of T_g is also conceivable for simple liquids with an attractive wall-particle interaction.

As a final remark we would like to stress the necessity of constructing microscopic mode coupling theories for the glass transition in fluids confined between two parallel plates that go beyond the simple law (24). Of course this is much more complicated than for the bulk problem since the structural input correlations are also more complicated. But, at least in principle, a construction of such a microscopic theory should be possible.

ACKNOWLEDGMENTS

We are indebted to J. L. Barrat, L. Bocquet, T. Palberg, and J. Jäckle for helpful discussions. This work was supported by the French-German PROCOPE exchange program under Contract No. 312-pro-93-as.

[1] J. P. Hansen, Phys. World **4** (12), 32 (1991).
[2] J. Van Alsten and S. Granick, Phys. Rev. Lett. **61**, 2570 (1988).
[3] H.-W. Hu, G. A. Carson, and S. Granick, Phys. Rev. Lett. **66**, 2758 (1991).
[4] *Molecular Dynamics in Restricted Geometries,* edited by J. Klafter and J. M. Drake (Wiley, New York, 1989).
[5] S. A. Somers and H. T. Davis, J. Chem. Phys. **96**, 5389

(1992).
[6] M. Schoen, J. H. Cushman, and D. J. Diestler, Mol. Phys. **81**, 475 (1994).
[7] P. A. Thompson, G. S. Grest, and M. O. Robbins, Phys. Rev. Lett. **68**, 3448 (1992).
[8] C. L. Jackson and G. B. McKenna, J. Non-Cryst. Solids **131-133**, 221 (1991).
[9] P. Pissis, D. Daoukaki-Diamanti, L. Apekis, and C. Christodoulides, J. Phys. Condens. Matter **6**, L325 (1994).
[10] J. Zhang, G. Liu, and J. Jonas, J. Phys. Chem. **96**, 3478 (1992).
[11] J. Dubochet, M. Adrian, J. Teixeira, C. M. Alba, R. K. Kadiyala, D. R. MacFarlane, and C. A. Angell, J. Phys. Chem. **88**, 6727 (1984).
[12] K. Hofer, E. Mayer, and G. P. Johari, J. Phys. Chem. **95**, 7100 (1991).
[13] J. Schüller, Y. B. Mel'nichenko, R. Richert, and E. W. Fischer, Phys. Rev. Lett. **73**, 2224 (1994).
[14] J. L. Keddie, R. A. L. Jones, and R. A. Cory, Europhys. Lett. **27**, 59 (1994).
[15] J. L. Barrat and M. L. Klein, Annu. Rev. Phys. Chem. **42**, 23 (1991).
[16] H. Löwen, Phys. Rep. **237**, 249 (1994).
[17] W. Götze, in *Liquids, Freezing and the Glass Transition,* edited by J. P. Hansen, D. Levesque, and J. Zinn-Justin (North-Holland, Amsterdam, 1991).
[18] P. Ray and K. Binder, Europhys. Lett. **27**, 53 (1994).
[19] B. Bernu, J. P. Hansen, Y. Hiwatari, and G. Pastore, Phys. Rev. A **36**, 4891 (1987).
[20] J. N. Roux, J. L. Barrat, and J. P. Hansen, J. Phys. Condens. Matter **1**, 7171 (1989).
[21] J. L. Barrat, J. N. Roux, and J. P. Hansen, Chem. Phys. **149**, 197 (1990).
[22] J. Matsui, T. Odagaki, and Y. Hiwatari, Phys. Rev. Lett. **73**, 2452 (1994).
[23] M. P. Allen and D. J. Tildesley, *Computer Simulation of Liquids* (Clarendon, Oxford, 1987).
[24] For more details see T. Fehr, Diploma thesis, University of Munich, 1994 (unpublished).
[25] T. Biben, R. Ohnesorge, and H. Löwen, Europhys. Lett. **28**, 665 (1994).
[26] S. Ranganathan and G. S. Dubey, J. Phys. Condens. Matter **5**, 387 (1993).
[27] S. Ranganathan, J. Phys. Condens. Matter **6**, 1299 (1994).
[28] L. Bocquet and J. L. Barrat, Phys. Rev. Lett. **70**, 2726 (1993).
[29] L. Bocquet and J. L. Barrat, Phys. Rev. E **49**, 3079 (1994).
[30] T. Geszti, J. Phys. C **16**, 5805 (1983).
[31] L. Bocquet and J. L. Barrat, Europhys. Lett. (to be published), and private communication.
[32] W. van Megan and S. M. Underwood, Phys. Rev. E **49**, 4206 (1994).
[33] C. A. Murray and D. H. van Winkle, Phys. Rev. Lett. **58**, 1200 (1987).
[34] C. A. Murray, W. O. Sprenger, and R. A. Wenk, Phys. Rev. B **42**, 688 (1990).
[35] D. G. Grier and C. A. Murray, J. Chem. Phys. **100**, 9088 (1994).
[36] W. Schaertl and H. Sillescu, J. Colloid Interface Sci. **155**, 313 (1993).
[37] K. Vondermaßen, J. Bongers, A. Mueller, and H. Versmold, Langmuir **10**, 1351 (1994).
[38] H. Löwen, J. Phys. Condens. Matter **4**, 10 105 (1992).
[39] H. Löwen, J. P. Hansen, and J. N. Roux, Phys. Rev. A **44**, 1169 (1991).
[40] G. Szamel and H. Löwen, Phys. Rev. A **44**, 8215 (1991).